THE VALIDATION OF CLOUD RETRIEVAL ALGORITHMS USING SYNTHETIC DATASETS

Alexander Kokhanovsky[(1)], Jürgen Fischer[(2)], Rasmus Lindstrot[(2)] , Jan Fokke Meirink[(3)], Caroline Poulsen[(4)], Rene Preusker[(2)] , Richard Siddans[(4)], Gareth Thomas[(5)], Chris Arnold[(5)], Roy Grainger[(5)], Luca Lelli[(1)], Vladimir Rozanov[(1)]

[(1)]Institute of Environmental Physics, Bremen University, O. Hahn Allee 1, D-28334 Bremen, Germany, Email: lsr@iup.physik.uni-bremen.de

[(2)]Institute of Meteorology, Free University of Berlin, Carl-Heinrich-Becker-Weg 6-10, 12165 Berlin, Germany Email: rasmus.lindstrot@wew.fu-berlin.de

[(3)] Royal Netherlands Meteorological Institute (KNMI), Climate Observations Department PO Box 201 , 3730 AE De Bilt, The Netherlands Email: jan.fokke.meirink@knmi.nl

[(4)] Rutherford Appleton Laboratory, Campus, Didcot, OX11 0QX, UK Email: caroline.poulsen@stfc.ac.uk

[(5)]Department of Physics, University of Oxford, Parks Road, Oxford, OX1 3PU, UK Email: gthomas@atm.ox.ac.uk

ABSTRACT

We have performed the inter-comparison study of cloud property retrievals using algorithms initially developed for AATSR (ORAC, RAL-Oxford University), AVHRR and SEVIRI (CPP, KNMI), SCIAMACHY/GOME (SACURA, University of Bremen), and MERIS (ANNA, Free University of Berlin). The accuracy of retrievals of cloud optical thickness (COT), effective radius (ER) of droplets, and cloud top height (CTH) is discussed.

INTRODUCTION

Retrieval of cloud properties from space is usually performed using 2-channel algorithms. The visible channel is used to estimate the cloud optical thickness and the channel in the near infrared (say, at 1.6 or 2.1 μm) is used to determine the effective size of droplets and crystals in clouds. Although the algorithms ideally must produce identical results if the same input data are used, this is often not the case due to different assumptions with respect to the cloud mask, refractive index of particles, types of droplet and crystal size spectra used, different surface albedo databases, assumptions on the shapes of particles, atmospheric state, and radiative transfer models. Therefore there is a need for understanding and quantifying the differences between various algorithms. Such an inter-comparison study was performed in the framework of the ESA Cloud_CCI Project(http://www.esa-cloud-cci.org/) and reported in this paper. The paper is structured as follows. In the next section we introduce the algorithms used. Then the synthetic dataset is presented. The final section describes the results of the inter-comparison study.

2. ALGORITHMS

2.1. Oxford RAL Aerosol and Cloud (ORAC) algorithm for ATSR, AVHRR and SEVIRI

The ORAC algorithm [1, 2] is an optimal estimation retrieval that can be used to determine both aerosol and cloud properties from visible/infrared satellite radiometers. In the case of cloud retrievals, the algorithm fits radiances (computed from LUTs created from DIScrete Ordinates Radiative Transfer (DISORT) code to the top/of/atmosphere (TOA) signal measured by the satellite) by varying the cloud optical thickness (COT), effective radius (ER), cloud top pressure and height, phase and surface temperature simultaneously. The result is a radiatively consistent set of cloud properties. The cloud retrieval has thus far been applied to ATSR-2 and AATSR, as well as to SEVIRI and AVHRR measurements; however it could easily be adapted to MODIS retrievals. ORAC uses real-time radiative transfer, a method which relies on fitting the measurements, to within expected error limits, to the predicted values. Since exact methods are far too slow, the strategy adopted is to utilise 'fast', non-exact, radiative transfer models with analytical gradients. This is achieved by decoupling the cloud and atmospheric ('cloudfree atmosphere') parts of the system. ORAC then uses precalculated multiple scattering cloud radiative properties stored in look-up tables (LUTs), and clear atmosphere radiance and transmission calculations (MODTRAN (http://www.modtran.org/), for the visible channels, and RTTOV (http://research.metoffice.gov.uk/research/interproj/nwpsaf/rtm/rttov_description.html) for the infrared region of the electromagnetic spectrum. ORAC also uses Mie scattering for water droplets and optical properties from [3] for ice crystals. The ORAC algorithm is based currently on a single layer cloud model and retrieves cloud optical thickness, cloud top pressure, cloud effective radius, and cloud

Proc. of 'ATMOS 2012 – Advances in Atmospheric Science and Applications', Bruges, Belgium (ESA SP-708, November 2012)

fraction for an assumed droplet size distribution $f(a) = Ba^{\mu}e^{-\mu a/a_0}$ with $\mu = 6$. The effective radius a_{ef} is related to the modal radius a_0 as: $a_{ef} = (1+3/\mu)a_0$ and B is the constant. The retrievals have an associated cost and error. From these retrieved products one can subsequently derive liquid and ice water paths.

2.2. KNMI CPP retrieval scheme for SEVIRI, AVHRR and MODIS

The Cloud Property Product (CPP) retrieval scheme, developed at KNMI, retrieves cloud optical thickness τ, cloud particle effective radius a_{ef}, cloud thermodynamic phase (CPH), and liquid/ice/total cloud water path (LWP/IWP/CWP). At present, daily and monthly mean COT, CPH and CWP are produced as official products within EUMETSAT's Satellite Application Facility on Climate Monitoring (CM-SAF), both for geostationary (MSG-SEVIRI) and polar-orbiting (NOAA/METOP-AVHRR) imagers. Application of CPP to MODIS is being performed for scientific studies. The retrieval scheme is based on earlier methods that retrieve cloud optical thickness and cloud particle size from satellite radiances at wavelengths in the non-absorbing visible and the moderately absorbing solar infrared part of the spectrum [4]. The principle of the CPP algorithm is that the reflectance of clouds at a non-absorbing wavelength in the visible region (VIS: 0.6 or 0.8 μm) is strongly related to τ and has little dependence on a_{ef}, whereas the reflectance of clouds at an absorbing wavelength in the near-infrared region (NIR: 1.6 or 3.9 μm) is primarily related to a_{ef}. Moreover, differences between the imaginary parts of the refractive indices of water and ice in the NIR allow the retrieval of CPH. LWP can be computed as LWP = 2 τ a_{ef} ρ/3, where ρ is the density of liquid water. IWP is retrieved with the same formula using the effective radius of ice crystals and density of ice. The CPP algorithm compares satellite observed reflectances at visible and near-infrared wavelengths to look-up tables (LUTs) of simulated reflectances for given cloud optical thicknesses, particle sizes and surface albedos for water and ice clouds. The Doubling Adding KNMI (DAK) radiative transfer model has been used to generate the LUTs of simulated cloud reflectances. DAK has been developed for line-by-line or monochromatic multiple scattering calculations at UV, visible and near infrared wavelengths in a horizontally homogeneous cloudy atmosphere using the doubling-adding method [5]. The clouds are assumed to be plane-parallel and embedded in a multi-layered Rayleigh scattering atmosphere. The particles of water clouds are assumed to be spherical droplets with effective radii between 1 and 24 μm. The size distribution is the same as for ORAC (see above) but $\mu = 11/3 \approx 3.7$ (or the effective variance $v_{ef} = (\mu+3)^{-1} = 0.15$). Therefore, the size distribution assumed in the CPP algorithm is broader compared to that assumed in ORAC. For ice clouds, homogeneous distributions of imperfect hexagonal ice crystals [6] are assumed with effective radii between 6 and 51 μm. It was demonstrated in [7] that these crystals give adequate simulations of total and polarized reflectances of ice clouds. The surface albedo over land is prescribed from an average of five years of MODIS white-sky albedo data, while over ocean a surface albedo of 0.05 is assumed for both the VIS and NIR channels. Atmospheric correction of the reflectances is performed using a LUT approach based on MODTRAN simulations [8, 9]. COT and ER are retrieved for cloudy pixels (determined from the cloud masking algorithm developed in [10]) in an iterative manner. During the iteration the retrieval of τ in the VIS channel is used to update the retrieval of a_{ef} in the NIR channel. This iteration process continues until the retrieved cloud physical properties converge to stable values (based on fixed criteria). The interpolation between cloud physical properties in the LUTs is done with polynomial interpolation for τ and linear interpolation for a_{ef}. The retrieved effective particle size is unreliable for optically thin clouds. Therefore, for COTs τ<8, assumed climatologically averaged effective radii of 8 μm and 26 μm for water and ice clouds, respectively, are used. To obtain a smooth transition between assumed and retrieved a_{ef} a weighting function is applied for clouds with τ<8. The gradients of the VIS and NIR reflectance with respect to τ and a_{ef} are used to calculate error estimates of the retrieved τ and a_{ef}. CPH is determined as follows. The iterative process described above is first applied using the ice cloud LUT. If convergence is achieved and the cloud-top temperature (CTT) is lower than 265 K, the phase 'ice' is assigned. If not, the phase 'water' is assigned, and the iterative process to find τ and a_{ef} is applied using the water cloud LUT. The cloud temperature is calculated from the 11-μm brightness temperature and the cloud emissivity. Validation of CPP algorithm products with ground-based observations has been performed in [11]. More details on the CPP algorithm are given in [9].

2.3. SCIAMACHY cloud retrieval algorithm

A Semi-Analytical CloUd Retrieval Algorithm (SACURA) developed at Bremen University is aimed at the determination of cloud liquid water path, effective radius of droplets and cloud optical thickness using spaceborne observations. The cloud top height is retrieved using measurement in the oxygen A-band. The algorithm is based on the asymptotical solution of the

radiative transfer equation for a special case of cloudy media, having a large optical thickness($\tau \geq 4$). The asymptotical solutions are further simplified such that the inverse problem is reduced to the solution of a single transcendent equation. This allows us to speed up the retrieval process significantly without substantial loss of accuracy of the retrieved parameters. The values of a_{ef} and LWP w are found from the system of two algebraic equations [12]:

$$R_1 = R_\infty^0 - \frac{t_1\left(a_{ef}, w\right)\left[1 - A_1\right]}{1 - A_1\left[1 - t_1\left(a_{ef}, w\right)\right]} K_0\left(\vartheta\right) K_0\left(\vartheta_0\right) \quad (1)$$

$$R_2 = R_\infty^0 \exp\Big(- y_2\left(a_{ef}\right)(1 - 0.05 y_2\left(a_{ef}\right))u \Big)$$

$$- \left[\exp(-x_2\left(a_{ef}, w\right) - y_2\left(a_{ef}\right)) - \frac{t_2\left(a_{ef}, w\right) A_2}{1 - A_2 r_2\left(a_{ef}, w\right)} \right]$$

$$\times t_2\left(a_{ef}, w\right) K_0\left(\vartheta\right) K_0\left(\vartheta_0\right), \quad (2)$$

where R_1 and R_2 are the measured reflection functions (t_1 and t_2 are the transmitivities) in the visible and infrared, respectively, r_2 is the cloud spherical albedo in the NIR, $u = K_0\left(\vartheta\right) K_0\left(\vartheta_0\right) / R_\infty^0$, R_∞^0 is the reflection function of a semi-infinite nonabsorbing cloud, and $K_0\left(\vartheta\right) = 3(1 + 2\cos\left(\vartheta\right)) / 7$. The subscripts "1 " and "2 " refer to wavelengths λ_1 and λ_2 in visible and near – infrared channels, respectively. Values of A_1 and A_2 are the surface albedos in the visible and near-infrared, respectively, ϑ_0 is the solar zenith angle(SZA), ϑ is the viewing zenith angle (VZA). Equations (1) and (2) are used to find two unknowns (a_{ef} and w) applying the parameterizations of local cloud optical parameters x_2, y_2 as functions of a_{ef} and w [12] .

2.4. MERIS cloud retrieval algorithm

The algorithm for the remote sensing of cloud-top pressure from MERIS measurements makes use of the absorption of solar radiation by oxygen at 0.76 μm by relating the strength of absorption to the transmitted airmass: the transmission decreases as the transmitted absorber mass increases. A wide field of remote sensing applications uses this differential absorption technique for the estimation of masses, e.g. the estimation of atmospheric water vapour or trace gases. The presence of clouds significantly alters the path lengths of reflected and backscattered photons, with high clouds leading to shorter path lengths and high transmission, and low clouds leading to longer path lengths and low transmission. The transmission cannot be measured directly, it is estimated by the ratio of the measured radiance in the absorption channel and one absorption-free window channel, namely MERIS channels 11 at 762nm and 10 at 754nm [13]. The enhancement of photon path lengths due to in-cloud multiple scattering is a function of cloud optical thickness. Therefore, the window radiance at 754nm serves as an additional input parameter to the algorithm, as it allows an estimation of the cloud optical thickness. Although the vertical profile of extinction and the cloud geometrical thickness are not known, the inclusion of the window channel radiance allows for the correction of multiple scattering effects within the cloud layer [14].

The above-described algorithm was implemented in the MERIS ground segment [15]. For reasons of computational efficiency, the inversion of the MERIS radiances is performed by an Artificial Neural Network Algorithm(ANNA), trained with a comprehensive simulation database. The radiative transfer code MOMO [16, 17] was used for the training database generation. In order to account for the influence of the reflecting surface on the average photon path length, globally mapped albedo values, generated from MERIS and MODIS data are used (ALBEDOMAP[18]). In the radiative transfer simulations used as a training database for the ANNA, the cloud extinction and droplet effective radius were varied within physically consistent limits, in order to represent the globally occurring variability. For example, the extinction was varied between low values of down to $2\ km^{-1}$ for cirrus clouds to up to $130\ km^{-1}$ for dense convective clouds.

Due to the lack of channels in the shortwave infrared and thermal infrared spectral regions, the measurements of MERIS do not provide enough information for a retrieval of liquid/ice water profiles and path. The cloud optical thickness can be derived from the window reflectance at 754nm, using the MERIS ALBEDOMAP database for the consideration of the surface reflectance, which is an important influence particularly in cases of optically thin clouds. The common simultaneous retrieval of optical thickness and effective droplet radius, as proposed in [4] and applied to, for example, MODIS or SEVIRI observations, cannot be applied to MERIS data, as it lacks a spectral channel at 1.6μm or 3.7μm. Instead, a climatologically averaged effective cloud droplet size is assumed in the retrieval algorithm. Consequently, the accuracy of the retrieved cloud optical thickness is limited. However, since the effective droplet radius from a Nakajima/King-like retrieval is only valid for a certain level close to the cloud-top while the vertical profile remains unknown, the MERIS retrieval scheme is not substantially inferior.

3. DESCRIPTION OF THE SYNTHETIC DATASET

The synthetic top-of-atmosphere reflectances (TOAR) have been simulated using the radiative transfer software package SCIATRAN [19]. Thirty six cloudy scenarios have been studied. The cases differed by cloud bottom height (CBH), cloud top height (CTH), effective radius of droplets, and cloud optical thickness. It was assumed that the droplet size distribution is given by the following function $f(a) = Ba^{\mu}e^{-\mu a/a_0}$ with $\mu = 6$ (the same as in ORAC). The task was to find cloud parameters such as CTH, COT, and ER from the simulated TOAR. The calculations have been performed at a solar zenith angle equal to 60 degrees, various viewing zenith angles and relative azimuths (RAA), underlying surface albedos and channels. Due to the reciprocity principle, the calculations at fixed SZA and various VZAs can be interpreted as those for a fixed VZA and varying SZA. Calculations at the following wavelengths have been performed: 555nm, 658nm, 753nm, 860nm, 1242nm, 1585nm, and 2114nm using the exponential sum fitting of transmissions (ESFT) approach implemented in SCIATRAN. The ESFT procedure has been applied to monochromatic calculations at predetermined reference pressure, temperature and gaseous absorber amount. In addition, to simulate MERIS measurements in the oxygen A-band, we have calculated TOAR in the vicinity of 760nm using the spectral MERIS instrument Spectral Response Function (SRF). To simulate the smile effect the RSF was shifted by 1.75nm and calculations have been performed for the central wavelength 761.75nm. We found that the influence of the particular choice of the instrument response function for other wavelengths is negligible. Therefore, monochromatic calculations at central wavelengths specified above have been performed. Radiances at the wavelengths 3.7 μm, 11 μm, and 12 μm have also been calculated assuming a surface emissivity of 0.95 and a surface temperature of 290K. It was assumed that absorption by both ozone and water vapour takes place in the atmosphere. Rayleigh scattering was fully taken into account using the parameterization presented in [20]. The scattering and absorption of light by particulate matter suspended in the atmosphere was neglected.

4. RESULTS OF RETRIEVALS

4.1. ORAC(Oxford-RAL)

The results of retrievals using ORAC and corresponding errors are given in Figures 1, 2. The channels at 0.55, 0.6, 0.87, 1.6, and 11 μm have been used for the simultaneous retrieval of ER, COT, and CTH. The relative error is calculated as: error=100*(retrieved-true)/true. The absolute error is defined as Δ = retrieved-true. The positive errors mean the overestimation of a corresponding parameter. It follows that the retrieval error is smaller than 5% for COT and 15% for ER in the case under study (the nadir observation at SZA=60°). The absolute relative error in COT is below 2.5% in most cases. It hardly changes with COT. The error in ER increases with the value of ER. In most cases it is below 10%. A part of this error is due to the fact that the forward models used in the simulation of ORAC LUTs differ from the SCIATRAN forward simulation performed in this work. In particular, it was assumed that the imaginary part of the complex refractive index χ is 0.0000855 in ORAC and it is 0.00009347 in forward SCIATRAN calculations. The value of χ is not very certain and depends on the presence of impurities inside the cloud droplets and also on temperature. This could contribute to the error in the retrieved value of ER (in particular, for larger radii, see Figure 2). However, one concludes from Figure 3 that generally errors of retrievals are negligible, especially if one takes into account the calibration errors and uncertainty in underlying surface reflectance, and also the deviation of a real cloud as observed in nature from the simplistic models used in the inversion procedure. As one might expect, errors grow for thinner clouds and also for larger droplets (see Figure 3). The absolute error in the retrieved cloud top height is generally below 0.5 km (an underestimation, especially for the case of geometrically thick clouds, see Figure 4). The error increases for optically thin clouds ($\tau \le 2$) and can reach 1.4km. In the case of multi-layered cloud systems ORAC retrieves the CTH of upper cloud and it is generally not sensitive to the clouds at lower levels. The errors grow with VZA and also with ground albedo (not shown here). In particular, at SZA=60 degrees and VZA=55 degrees the absolute value of the maximal error in COT is 5% and it is 20% in ER for the cases considered. The error can reach 60% at the backscattering geometry, where RAA=180 degrees. Clearly, the nadir observation mode of AATSR is more suitable for retrievals.

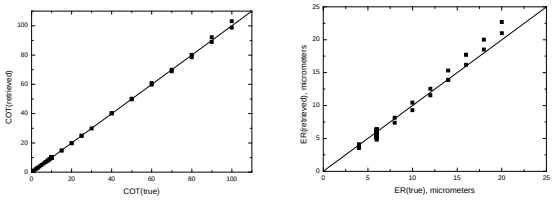

Figure 1. The correlation between retrieved and assumed cloud parameters for the studied cases at SZA=60°, VZA=0°, 55° and black underlying surface. The cases with VZA=55° have larger retrieval errors.

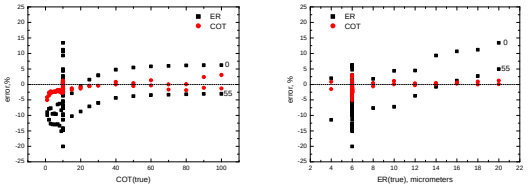

Figure 2. The errors of ORAC retrievals for the cases presented in Appendix 1 at SZA=60°, VZA=0° and 55° for the black underlying surface. The absolute value of the relative error is below 20% for all cases considered.

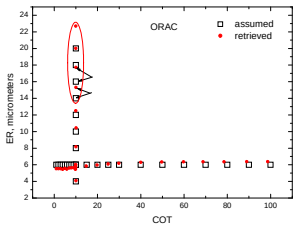

Figure 3. The dependence of the effective radius on COT for 36 cases as derived from ORAC (red symbols) and in the synthetic dataset (black symbols). The input parameters are the same as in Figure 1 except for the nadir observation. The deviations for larger radii are due to slightly different assumptions on the complex refractive index of water in SCIATRAN and ORAC.

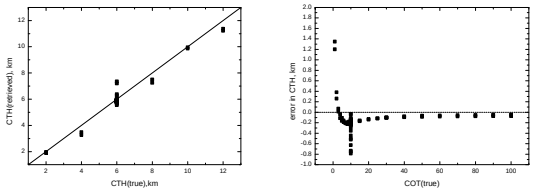

Figure 4. The results of ORAC retrievals of cloud top height and, respectively, absolute errors. The input parameters are the same as in Figure 1. Errors increase for the optically thin clouds ($\tau \le 2$).

4.2. CPP algorithm (KNMI)

The results of retrievals using the CPP algorithm for the same setup as in Figure 1, and corresponding errors, are presented in Figure 5. The channels 0.6 and 1.6 μm have been used. The errors are larger as compared to the ORAC retrievals. They reach 12% for COT and 22% for ER. This is related to the fact that the effective variance of the droplet size distribution assumed in the CPP retrieval was different from that used in forward SCIATRAN runs and ORAC retrievals. Also, the imaginary part of the refractive index of water χ at wavelength 1.6 μm was assumed to be 0.0000822 in the CPP algorithm LUTs (not 0.00009347 as in the SCIATRAN forward modeling). In addition, although in SCIATRAN forward calculations only the O2, O3, and H2O gases were included, the CPP algorithm also assumed that CH4 and CO2 gases were present. The CTH of 2km was assumed in the retrievals. The aerosol scattering was not switched off in the retrievals. All these factors contributed to biases in retrievals. It follows that the uncertainty in the effective variance on the retrievals has a greater influence for thicker clouds, where reflectance becomes generally less sensitive to the change of COT. The uncertainty in χ is also of greater importance for larger particles. For most cases, the retrieval error for COT is smaller than 10% and it is smaller than 15% for ER, which is suitable for practical applications of the method (see Figures 5a,b). It follows from Figure 5c that the error is larger for larger VZA (and also SZA). It increases at RAA=0 and 180 degrees (see Figure 5d). This is related to larger differences in the cloud phase functions in the forward simulation and in the retrieval procedure at these geometries. We also found that the errors remain below 20% in most cases at the surface albedo A=0.4 (not shown here).

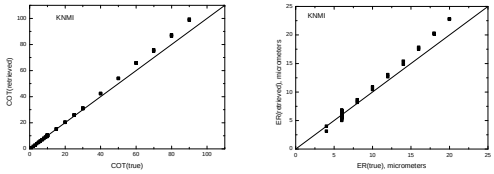

Figure 5a. The results of CPP retrieval. Input data are the same as in Figure 1. The CPP feature, which relies on the climatological values of ER for thin clouds, was switched off.

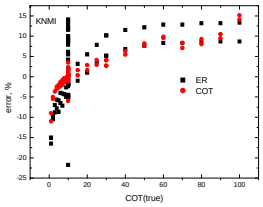

Figure 5b. The errors for retrievals shown in Figure 5a.

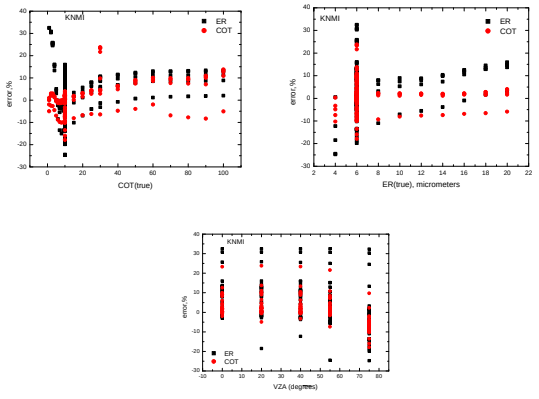

Figure 5c. The results of CPP retrievals and respective errors for various VZAs and SZA=60 degrees, RAA=90 degrees.

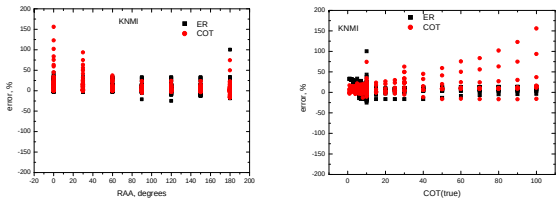

Figure 5d. The results of CPP retrievals and respective errors for various RAAs at SZA=60 degrees and VZA=0, 55 degrees.

4.3. SACURA (UB)

The retrievals using SACURA for the same setup as shown in Figure 1 (except at the nadir direction) are presented in Figures 6 and 7. The channels 0.865 and 1.6 μm have been used. The errors in COT are smaller than 20% at $\tau \geq 4$. SACURA is not applicable to thinner cloud, where it is assumed that $\tau = 2$ and $a_{ef} = 6 \mu m$. The error in ER is below 25%. It follows that errors of SACURA are somewhat larger as compared to those of ORAC. It follows from Figure 8 that the accuracy of SACURA is also acceptable for non-black underlying surfaces. In addition, the SACURA algorithm is much faster as compared to ORAC. Therefore, SACURA can be implemented as a first guess to other cloud retrieval algorithms. This will speed up the retrieval process considerably.

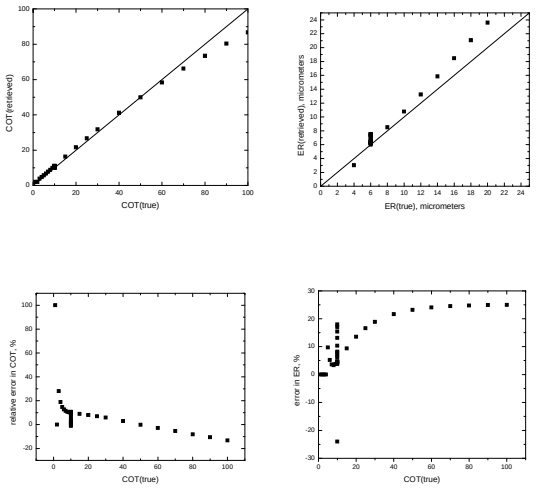

Figure 6. The results of SACURA retrievals and respective errors.

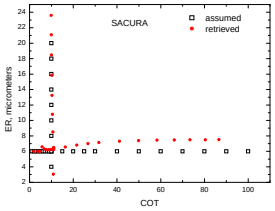

Figure 7. The dependence of the effective radius on COT for 36 cases as derived from SACURA (red symbols) and those in the synthetic dataset (black).

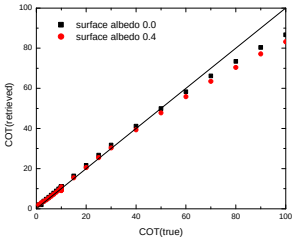

Figure 8. The SACURA retrievals at various values of albedo A of underlying surface.

4.4. ANNA (MERIS)

The results of retrievals using the MERIS algorithm for the determination of COT and CTH are presented in Figures 9 and 10, respectively. It follows from Figure 9 that the error for COT determination is below 30% in most cases considered ($COT \geq 3$). This is acceptable, taking into account that the MERIS measurements are not performed at 1.6 μm and, therefore, the size of droplets can not be determined and must be assumed in advance of retrievals. The errors of CTH retrieval are generally smaller than 1km. The average error is somewhat larger as compared to the ORAC algorithm, which is related to the fact that measurements are performed just for one broad channel in the oxygen A-band. In most cases, the CTH is overestimated and errors increase with the geometrical thickness of clouds. The results shown in Figures 9 and 10 are for the nadir observation and SZA=60 degrees. The influence of illumination and observation geometry on the retrievals is given in Figure 11. It follows that the error in CTH can grow up to 1.5km. Depending on the case, overestimation and underestimation are possible. The error in CTH depends on the cloud geometrical thickness. The errors are generally below 0.8km for 1km-thick clouds. However, there is a large CTH underestimation in the case of geometrically thick (3km) clouds. The retrieved COT is often not reliable. Generally, too thick clouds are retrieved (see Figure 11) for low sun (and large VZA). The results of retrievals at several surface albedo values are shown in Figure 12. It follows that low clouds are retrieved with higher accuracy as compared to high clouds. Generally, retrievals for optically thinner clouds (small

reflectances) lead to larger errors (see Figure 13). The errors are larger for geometrically thick clouds as compared to thinner (1km) clouds.

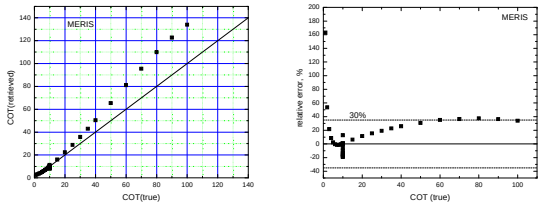

Figure 9. The results of MERIS algorithm retrievals and respective errors for the 36 cloud scenarios at SZA=60 degrees and nadir observation.

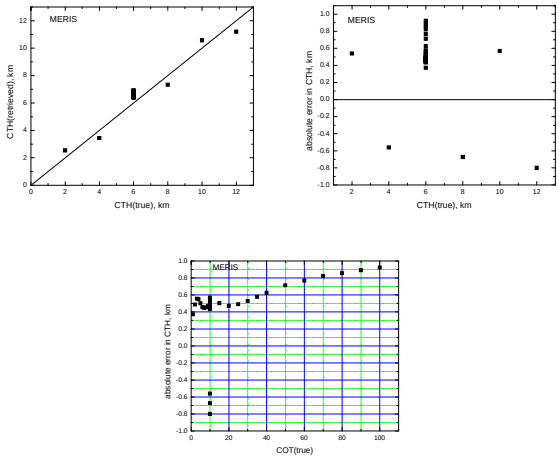

Figure 10. The same as in Figure 9 except for CTH. The negative errors for three cases as seen in the figure correspond to geometrically thick clouds (thickness – 3km).

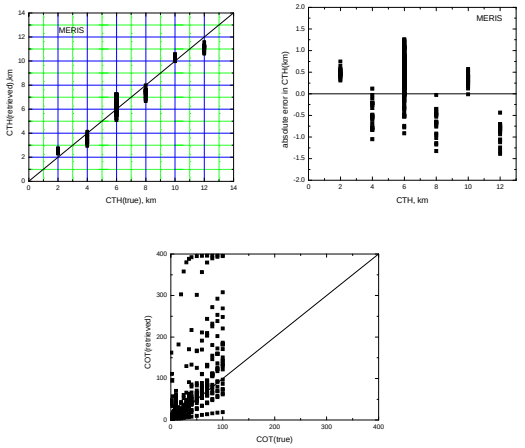

Figure 11. Errors in COT and CTH for the same cases as in Figure 9 except for varied viewing and illumination geometries (SZA=0, 20, 40, 60, 75 degrees and VZA=0, 20, 40, 55, 75 degrees for RAA=0, 90, 180). The surface albedo is 0.0.

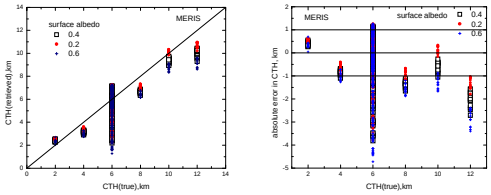

Figure 12. The results of retrievals and errors in CTH for the same as case as in Fig. 9 but for surface albedos of 0.2, 0.4, 0.6.

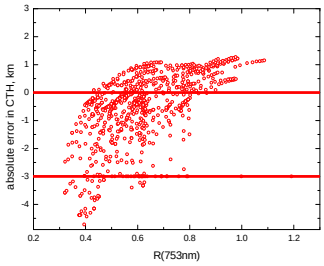

Figure 13. Errors in CTH for the same a case as in Figure 12 but for surface albedo of 0.4 only and as the function of top-of-atmosphere reflectance at 753nm.

5. CONCLUSIONS

Summing up, it follows that the theoretical errors of the pair (a_{ef}, τ) determination using the described algorithms for the range of input parameters considered are below 25% for ORAC, CPP and SACURA algorithms at nadir observation, black underlying surface and SZA=60 degrees. Errors of the algorithms grow with surface albedo and VZA. SACURA can be applied for clouds with COT larger than 4. The CTH is found with accuracy better than 0.8km for ORAC (except for COT=1, where errors are in the range 1.2-1.4km depending on the VZA) and 1km for MERIS at nadir observation and SZA=60 degrees. For larger variation of geometries and underlying surface albedos MERIS CTH has lower accuracy for high clouds (underestimation). The MERIS COT is often overestimated. The errors are larger for clouds having larger geometrical thickness. The errors can be reduced if the synergy of AATSR - MERIS observations is used. The errors of CPP retrieval are larger as compared to ORAC retrievals because SCIATRAN forward settings were adjusted to the ORAC and not to the CPP retrieval.

6. ACKNOWLEDGEMENTS

This work was supported by the ESA Project CLOUD_CCI. Oxford co-authors acknowledge support from the NERC National Centre for Earth Observation. University of Bremen co-authors thank the ESA Project SCIALOV for the support of this work.

7. REFERENCES

1. Poulsen, C. A., P. D. Watts, G. E. Thomas, A. M. Sayer, R. Siddans, R. G. Grainger, B. N. Lawrence, E. Campmany, S. M. Dean, and C. Arnold (2011). Cloud retrievals from satellite data using optimal estimation: evaluation and application to ATSR, *Atmos. Meas. Tech. Discuss.*, 4, 2389-2431.

2. Watts P.D., Mutlow C.T., Baran A.J. and Zavody A.M. (1998). Study on cloud properties derived from Meteosat Second Generation Observations. Eumetsat Report(http://www.eumetsat.de/en/area2/publications/rep_cloud.pdf).

3. Baran, A., et al. (2005). On the scattering phase function of non-symmetric ice crystals, *Q. J. R. Meteor Soc*, 131, 260916.

4. Nakajima, T. and M. D. King (1990). Determination of the optical thickness and effective particle radius of clouds from reflected solar radiation measurements. Part I: Theory. *J. Atmos. Sc*i., 47, 1878–1893.

5. De Haan, J. F., P. Bosma, and J. W. Hovenier (1987). The adding method for multiple scattering calculations of polarized light, *Astron. Astrophys*., 183, 371-391.

6. Hess, H, R. B. A. Koelemeijer, and P. Stammes (1998). Scattering matrices of imperfect hexagonal crystals, *J. Quant. Spectrosc. Radiat. Transfer*, 60, 301–308.

7. Knap, W. H., L. C. Labonnote, G. Brogniez, and P. Stammes (2005). Modeling total and polarized reflectances of ice clouds: evaluation by means of POLDER and ATSR-2 measurements, *Appl. Optics*, 44, 4060-4073.

8. Berk, A., L. S. Bernstein, and D. C. Robertson (1989). MODTRAN: A moderate resolution model for LOWTRAN 7. Technical Report GL-TR-89-0122, Geophysics Directorate, Phillips Laboratory, Hanscom AFB, MA 01731, USA.

9. Meirink, J.F., R. Roebeling, E. Wolters and H. Deneke (2010). Cloud Physical Products AVHRR / SEVIRI, Algorithm Theoretical Basis Document Document external project: 2010, EUMETSAT SAF/CM/KNMI/ATB D/CPP 1.0

10. Dybbroe, A., A. Thoss and K.-G. Karlsson (2005). NWCSAF AVHRR cloud detection and analysis using dynamic thresholds and radiative transfer-modeling - Part I: Algorithm description, *J. Appl. Meteor. Clim.*, 44, 39-54.

11. Roebeling, R.A., H. M. Deneke, and A. J. Feijt (2008). Validation of cloud liquid water path retrieveals from SEVIRI using one year of CloudNET observations, *J. Appl. Meteorol. Clim*., 47, 206-222.

12. Kokhanovsky, A. A. et al. (2003). A semianalytical cloud retrieval algorithm using backscattered radiation in 0.4-2.4 μm spectral region, *J. Geophys. Res.*, D108, 4008, doi: 10.1029/2001JD001543.

13. Preusker, R., and R. Lindstrot (2009). Remote sensing of cloud-top pressure using moderately resolved measurements within the oxygen A-band: A Sensitivity Study. *J. Appl. Meteor. Clim.*, 48, 1562–1574.

14. Fischer, J. and H. Grassl (1991). Detection of cloud-top height from backscattered radiances within the Oxygen A Band. Part 1: Theoretical study, *J. Appl. Meteor. Clim.*, 30, 1245–1259.

15. Fischer, J.; Preusker, R. & Schüller, L. (1997). ATBD 2.3 Cloud Top Pressure, European Space Agency.

16. Fischer, J. and Grassl, H. (1984). Radiative transfer in an atmosphere-ocean system: an azimuthally dependent matrix-operator approach, *Appl. Opt., 23*, 1035-1039.

17. Fell, F. & Fischer, J. (2001). Numerical simulation of the light field in the atmosphere-ocean system using the matrix-operator method, *J. Quant. Spectrosc. Radiat. Transfer*, 3, 351-388.

18. Muller, J.-P., Preusker, R., Fischer, J., Zuhlke, M., Brockmann, C., and Regner, P. (2007). ALBEDOMAP: MERIS land surface albedo retrieval using data fusion with MODIS BRDF and its validation using contemporaneous EO and in situ data products *IGARSS International Geoscience and Remote Sensing Symposium, 2007, IEEE International,* 2404-2407.

19. Rozanov, V. V., et al. (2012). SCIATRAN, *J. Quant. Spectr. Rad. Transfer*, in preparation.

20. Bates, D. R. (1984). Rayleigh scattering by air, *Planet. Space Sci*., 32, 785-790.